AGH DRILLING, OIL, GAS • Vol. 36 • No. 1 • 2019

http://dx.doi.org/10.7494/drill.2019.36.1.93

Danzhu Zheng*, Stefan Miska*, Małgorzata Ziaja*, Jianguo Zhang**

STUDY OF ANISOTROPIC STRENGTH PROPERTIES OF SHALE

Abstract: Shale has been known to be the source of wellbore instability during the drilling process. Organic rich shales are anisotropic due to their laminated structure and chemical properties. The goal of this study is to evaluate anisotropic mechanical properties of shale by triaxial tests, and predict shale anisotropic properties by well logging data interpretation. Shale samples were prepared with bedding plane inclination angles equal to 0 degrees, 45 degrees, and 90 degrees. Young's modulus, shear modulus, and Poisson's ratio in different directions were measured for a sample with 0 degrees bedding plane inclination angle. Parameters of the stiffness tensor were calculated by mechanical properties. Compressive strength was measured under different confining pressures of 0 psi, 500 psi, 1000 psi, and 1500 psi. The strength properties of shale samples were evaluated by both compressive strength and tensile strength. Simple Plane of Weakness and Modified Cam Clay failure criteria were applied to describe shear failure mechanisms. A scanning electron microscope method was used for the comparison of micro structures between the intact shale sample and failed sample with different bedding plane inclination angles. Well logging data was used to connect experimental lab data and field data. Compressional wave velocity was predicted with different inclination angles by stiffness parameters. The predicted compressional wave velocity for a 45-degree inclination angle showed a perfect fit with the field logging data. Steps of inverse sonic log data to stiffness parameters were shown by a flow chart. The UCS strength for 0 degrees and 45 degrees was predicted by several empirical relations using sonic logging data. The safe mud window for this special shale formation is predicted by experimental data. As shown in experimental results, our shale sample has a weak direction for both failure criteria. Well logging data and experimental data can be connected, especially by sonic log data. However, to predict shale anisotropic strength through well logging still requires more effort. The novelty of the process which connects experimental results and well logging data will be helpful for solving instability problems occurring in shale formation.

Keywords: shale rocks, anisotropic materials

* The University of Tulsa Drilling Research Projects
** British Petroleum

1. INTRODUCTION

The term shale is normally used for the entire class of fine-grained sedimentary rocks that contain substantial amount of clay minerals [1]. During the process of compaction and diagenesis, the platy shape of clay is usually distorted and has the tendency to be aligned in a parallel orientation. The specific type of paralleled layers make shale a laminated structure rock. Generally, reservoirs are assumed to be isotropic for simplicity. However, this assumption can be very dangerous in shale formation. Shale anisotropy, which related to inclination of the formation, is caused by the shale intrinsic lamination in various scales as well as the existence of preferred orientation of micro-fractures [2]. Anisotropy affects various properties of shales such as tensile strength [3], compressive strength, permeability [4] and sonic properties [5–8]. Shale exhibits isotropic properties within the bedding plane and different properties in the direction perpendicular to the bedding plane. As discussed by Lee [9], direction of breakout and wellbore stability analyses can be affected by anisotropic mechanical properties.

In the drilling industry, shale geo-mechanical properties can be predicted either by rock mechanics testing procedures or by empirical relations using well logging data. The accurate evaluation of anisotropic geo-mechanical properties for shale not only help with mitigating drilling issues, but also help to reduce non-productive time.

The procedures of rock mechanics testing require use of relatively large samples, with diameter and length dimensions of 5.08 cm by 10.16 cm (2 inch by 4 inch) or 2.54 cm by 5.08 cm (1 inch by 2 inch) in laboratory. The other way of predicting shale geo--mechanical properties by empirical correlations, is by extensive laboratory testing of shale cores. The basis for these relations is the fact that many of the same factors that affect rock properties also affect other physical properties such as velocity, elastic moduli and porosity [10]. As recommended by Per et al. 2011 [11], shale geo-mechanical properties can be predicted from various sources such as sonic wireline log, MWD sonic, and acoustic measurement on cuttings.

By connecting both the experimental and well logging interpretation, the objectives of this research are not limited to study shale geo-mechanical properties, but also extend the study to the anisotropic nature of shales, especially to diagnose the anisotropic strength of shales.

2. BRIEF REVIEW OF TRANSVERSE ISOTROPY

Transversely isotropic material is one with physical properties that are symmetric about an axis and normal to a plane of isotropy. This transverse plane has infinite planes of symmetry and thus, within this plane, material properties are the same in all direc-

tions. For shale, the isotropy plane is generally the bedding plane. In the bedding plane, geo-mechanics properties are assumed the same in all directions.

Transverse isotropic nature reduces the number of independent elastic constants in the stiffness tensor. Thus, there are only five independent elastic constants among twelve nonzero components. Using Vigot et al. notation [12], the stiffness matrix for transverse isotropic material is:

$$\boldsymbol{C} = \begin{bmatrix} C_{11} & C_{12} & C_{13} & 0 & 0 & 0 \\ C_{12} & C_{11} & C_{13} & 0 & 0 & 0 \\ C_{13} & C_{13} & C_{33} & 0 & 0 & 0 \\ 0 & 0 & 0 & C_{44} & 0 & 0 \\ 0 & 0 & 0 & 0 & C_{44} & 0 \\ 0 & 0 & 0 & 0 & 0 & (C_{11} - C_{12})/2 \end{bmatrix} \tag{1}$$

The compliance matrix (inverse of stiffness matrix) in geomechanics parameters is:

$$\boldsymbol{C}^{-1} = \begin{bmatrix} \frac{1}{E_x} & -\frac{v_{yx}}{E_x} & -\frac{v_{zx}}{E_z} & 0 & 0 & 0 \\ -\frac{v_{xy}}{E_x} & \frac{1}{E_x} & -\frac{v_{zx}}{E_z} & 0 & 0 & 0 \\ -\frac{v_{xz}}{E_x} & -\frac{v_{xz}}{E_x} & \frac{1}{E_z} & 0 & 0 & 0 \\ 0 & 0 & 0 & \frac{1}{G_{yz}} & 0 & 0 \\ 0 & 0 & 0 & 0 & \frac{1}{G_{yz}} & 0 \\ 0 & 0 & 0 & 0 & 0 & \frac{2\left(1+v_{xy}\right)}{E_x} \end{bmatrix} \tag{2}$$

3. FAILURE CRITIERIA FOR ANISOTROPIC MATERIALS

3.1. Simple plain of weakness theory

The simple plane of weakness model was proposed by Jaeger and Cook [13]. The simple plane of weakness model supposes that anisotropic material is an isotropic body.

Inherent strength is the same in all directions, except for one set of parallel planes where the strength is lower. Since the paralleled bedding planes in shales may be planes of weakness, this model has a physical basis, and it is therefore quite important despite its simplicity. Failure in a rock matrix and along the weakness planes are described by the Mohr–Coulomb failure criterion. Material failure can take place either in the rock matrix or along these weak planes as a function of loading orientation [13]. The inherent shear stress in the planes of weakness is S_w and μ_w is the coefficient of internal friction. Experimental results by Donath [14], Hoek [15] and Jaeger [16], all show general behavior of the weak plane in anisotropic rocks.

According to Mohr–Coulomb-type failure criteria, weak planes to fail at a lower stress than that expected for intact rock. Consider a $\tau - \sigma$ plot for a shale, as illustrated in Figure 1. The illustrated stress configuration represents the lowest strength for failure.

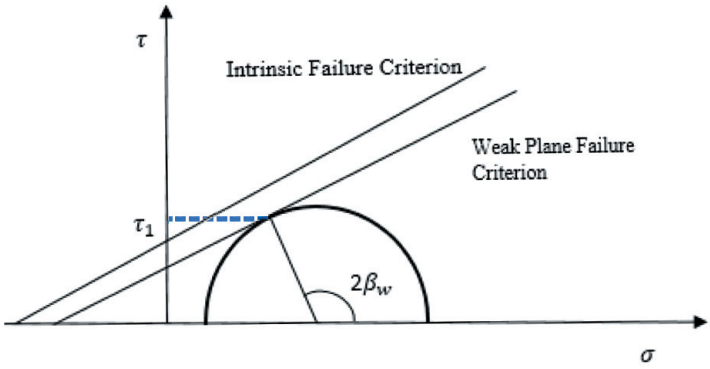

Fig. 1. Plot for shale containing a plane of weakness

The weak plane criterion is given by the cohesion factor as S_{0w} (intercept of the weak plane failure line and τ axis) and the friction angle is φ_w. The corresponding failure angle is:

$$\beta_w = \frac{\pi}{4} + \frac{\phi_w}{2} \tag{3}$$

The strength of the weak planes is given by eq. (4) [6]:

$$\sigma_1 - \sigma_3 = 2\,\frac{S_w \cos\varphi_w + \sigma_3 \sin\varphi_w}{\sin 2\theta \cos\varphi_w - (\cos 2\theta + 1)\sin\varphi_w} \tag{4}$$

The angle θ is the inclination angle; i.e., the angle between major principle stress and the normal to the weak plane. Angle θ is described by Figure 2.

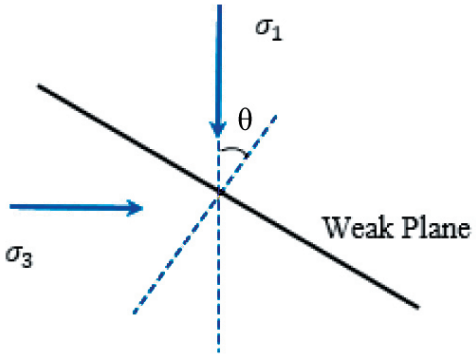

Fig. 2. Definition of inclination angle θ

The isotropic failure criterion (inherent cohesion S_0, corresponding to the friction angle φ) is described by:

$$\sigma_1 - \sigma_3 = 2\,\frac{S_o \cos\varphi + \sigma_3 \sin\varphi}{1 - \sin\varphi} \tag{5}$$

3.2. Modified Cam–Clay model

The Cam–Clay and Modified Cam–Clay models developed for normally consolidated clays under hydrostatic loading is the earliest model employed computationally [17]. Subsequently, many modified forms have been proposed to accommodate more general stress paths and soil types. The usage of the Modified Cam–Clay model has been extended to sand and weakly cemented sandstones [18, 19]. In this study, we will use the Modified Cam–Clay model. The yield function is given by eq. (6):

$$\Phi\left(\sigma, \varepsilon_v^p\right) = \left(\frac{q}{p}\right)^2 + M^2\left(1 - \frac{p_o}{p}\right) = 0 \tag{6}$$

where:

p – mean stress,
q – stress deviator,
p_o – pre-consolidation pressure.

The constant M defines the ratio between the two radii of the ellipsoid. The line with slope M is called the critical state line. Plots of the Cam–Clay model and Modified Cam–Clay model are shown in Figure 3.

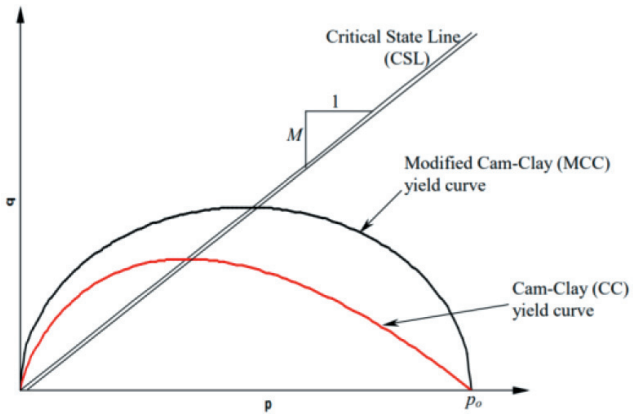

Fig. 3. Cam–Clay and Modified Cam–Clay models yield surface

4. EXPERIMENTAL RESULT

4.1. Triaxial tests for elastic properties

To obtain the stiffness tensor, the sample of 0 degrees bedding plane inclination angle was used. Two tests are performed with confining pressure of 3000 psi (20.68 MPa). The first test (see Figs. 4–6) was triaxial compression drained test. The second test (see Figs. 7–9) was the uniaxial radial strain drained test.

We design this special test to simulate the downhole condition. Parameters in the stiffness tensor will provide solid data for calculating the in-situ Young's modulus and Poisson's ratio. Meanwhile, these parameters are significant for computing the in-situ sonic velocity. Simulation of downhole condition in triaxial tests will provide a more accurate prediction of rock properties.

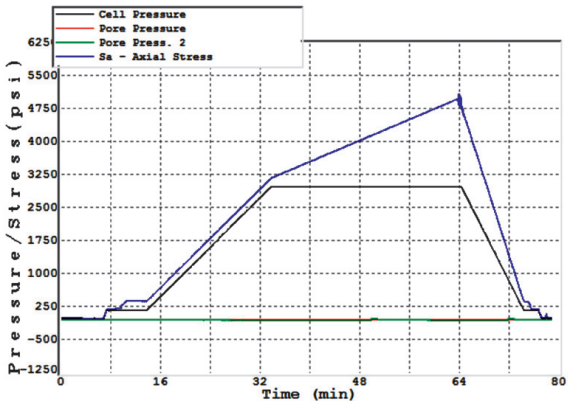

Fig. 4. Stress change versus time

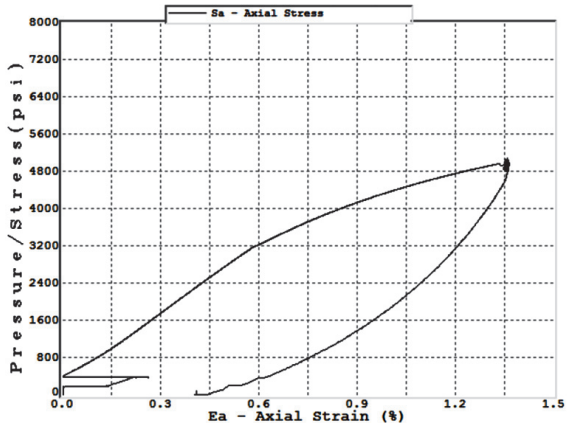

Fig. 5. Axial stress σ_a versus axial strain ε_a

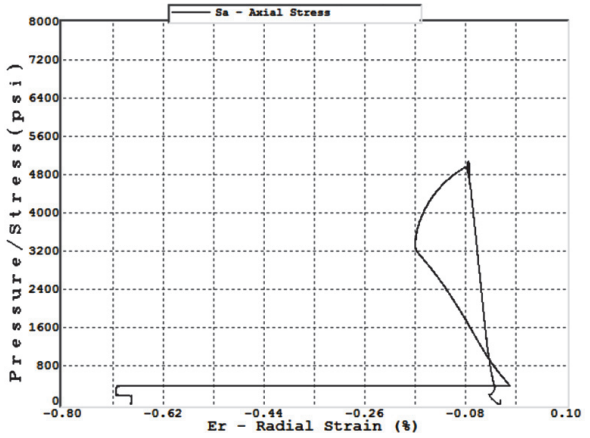

Fig. 6. Axial stress σ_a versus radial strain ε_r

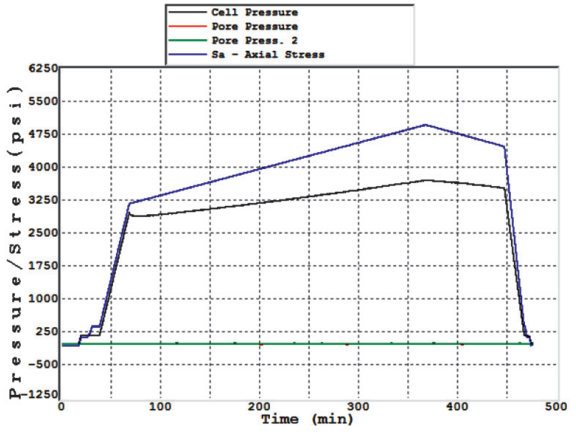

Fig. 7. Stress change versus time

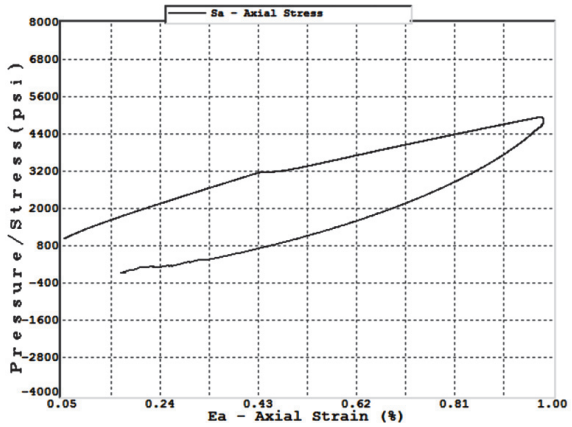

Fig. 8. Axial stress σ_a versus axial strain ε_r

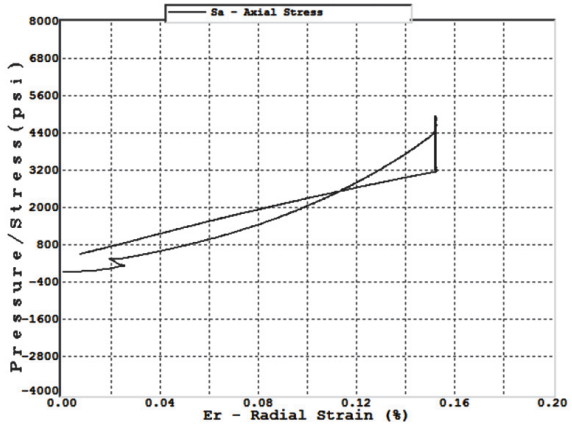

Fig. 9. Axial stress σ_a versus radial strain ε_r

According to Hook's law, the elastic parameters for Trinidad shale sample are listed in Table 1.

Table 1

Shale sample properties from Triaxial Test and Uniaxial Strain Test

Vertical Young's modulus E_V [GPa]	2.3
Vertical Young's modulus E_V [psi]	$3.34 \cdot 10^5$
Poisson's ratio rerpendicular to bedding plane υ_{rz} and $\upsilon_{\theta z}$	0.11
Horizontal Young's modulus E_H [GPa]	7.5
Horizontal Young's modulus E_H [psi]	$1.09 \cdot 10^6$
Poisson's ratio within bedding lane $\upsilon_{r\theta}$	0.35

We also obtained the compliance tensor and stiffness tensor as given by eqs. (7) and (8):

$$\boldsymbol{C}^{-1} = \begin{bmatrix} 0.13 & -0.047 & -0.02 & 0 & 0 & 0 \\ -0.047 & 0.13 & -0.02 & 0 & 0 & 0 \\ -0.02 & -0.02 & 0.435 & 0 & 0 & 0 \\ 0 & 0 & 0 & 1 & 0 & 0 \\ 0 & 0 & 0 & 0 & 1 & 0 \\ 0 & 0 & 0 & 0 & 0 & 0.36 \end{bmatrix} \tag{7}$$

$$\boldsymbol{C} = \begin{bmatrix} 8.99 & 3.34 & 0.57 & 0 & 0 & 0 \\ 3.34 & 8.99 & 0.57 & 0 & 0 & 0 \\ 0.57 & 0.57 & 2.35 & 0 & 0 & 0 \\ 0 & 0 & 0 & 1.00 & 0 & 0 \\ 0 & 0 & 0 & 0 & 1.00 & 0 \\ 0 & 0 & 0 & 0 & 0 & 2.78 \end{bmatrix} \tag{8}$$

Thomsen L. [5] proposed idea of parameterization of the elastic properties of a transversely isotropic medium to elaborate on diagnostic principles leading to a better understanding of anisotropy from isotropy. Thomsen's anisotropic parameters are calculated by the following eqs. (9), (10) and (11):

$$\varepsilon = \frac{C_{11} - C_{33}}{2C_{33}} \tag{9}$$

$$\gamma = \frac{C_{66} - C_{44}}{2C_{44}} \tag{10}$$

$$\delta = \frac{(C_{13} + C_{44})^2 - (C_{33} - C_{44})^2}{2C_{33}(C_{33} - C_{44})} \tag{11}$$

The Thomsen parameters for Trinidad shale are listed in Table 2. According to our calculation, ε is larger than one. This means that the shale sample is anisotropic of different bedding inclination angles.

Table 2

Thomson anisotropy parameters for Trinidad shale

ε	1.41
γ	0.89
δ	0.10

4.2. Compressive strength

The compressive strength for the shale was diagnosed by various confining pressures and different bedding inclination angles. Figure 10 depicts compressive strength as a function of confining pressure for the bedding inclination angle of 0 degrees. Figure 11 depicts compressive strength as a function of confining pressure for bedding inclination angle of 45 degree. From these figures, the compressive strength increases for both bedding inclination angles, with increasing confining pressures from 0 psi to 1500 psi. From Figure 10 and 11, we noticed that Young's modulus of 0 degrees bedding inclination angle of Trinidad shale increases as the confining pressure increases. However, the increment of confining pressure shows little influence at 45 degrees bedding inclination angle.

Figure 12 shows the comparison of compressive strength between different bedding inclinations. Meanwhile, the comparison is done with respect to different confining pressures. As shown in Figure 12, for the same bedding inclination angle, the higher the confining pressure the higher the compressive strength. Meanwhile, we notice that the compressive strength at 0 degrees bedding inclination angle is higher than that at 45 degrees.

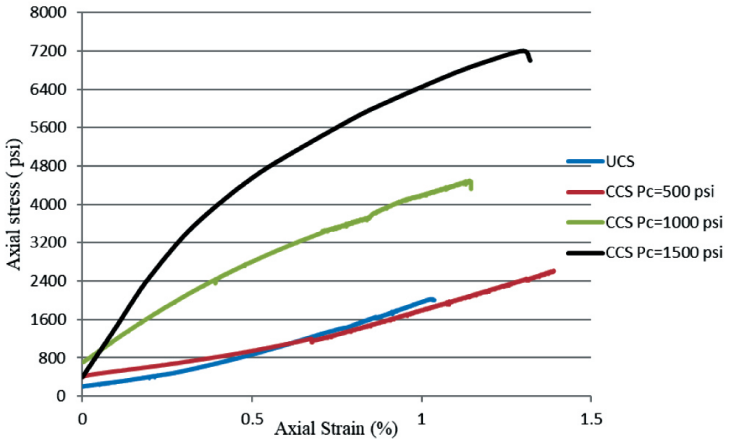

Fig. 10. Compressional strength versus confining pressure for 0 degrees bedding inclination angle

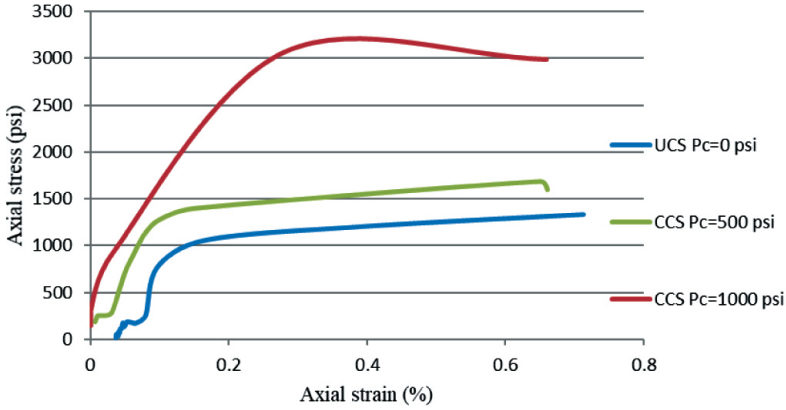

Fig. 11. Compressive strength versus confining pressure for 45 degrees bedding inclination angle

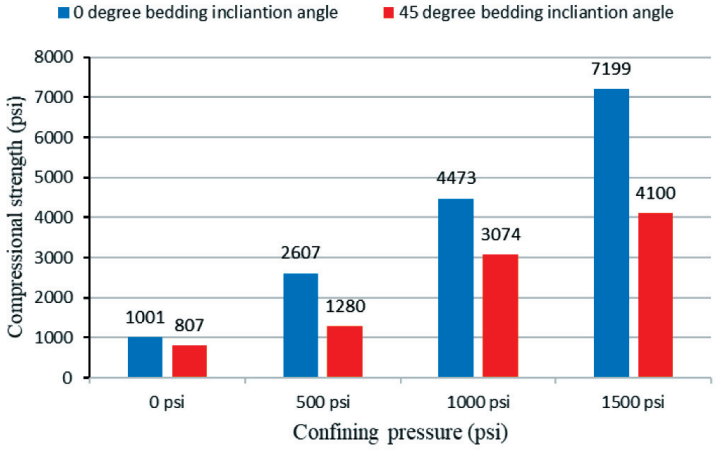

Fig. 12. Compressive strength of various bedding inclination angles under tri-axial conditions

4.3. Failure criterion

Simple plain of weakness model

Figures 13a to 13c show us different failure envelopes for the Trinidad shale. We observed that according to experimental data, two failure envelops were plotted.

Another plot of $(\sigma_1 - \sigma_3)$ versus the inclination angle is shown in Figure 14. Real failure results (round points) according to lab tests are also plotted.

The data of material constants, the R-squared and RMSE are presented in Table 3.

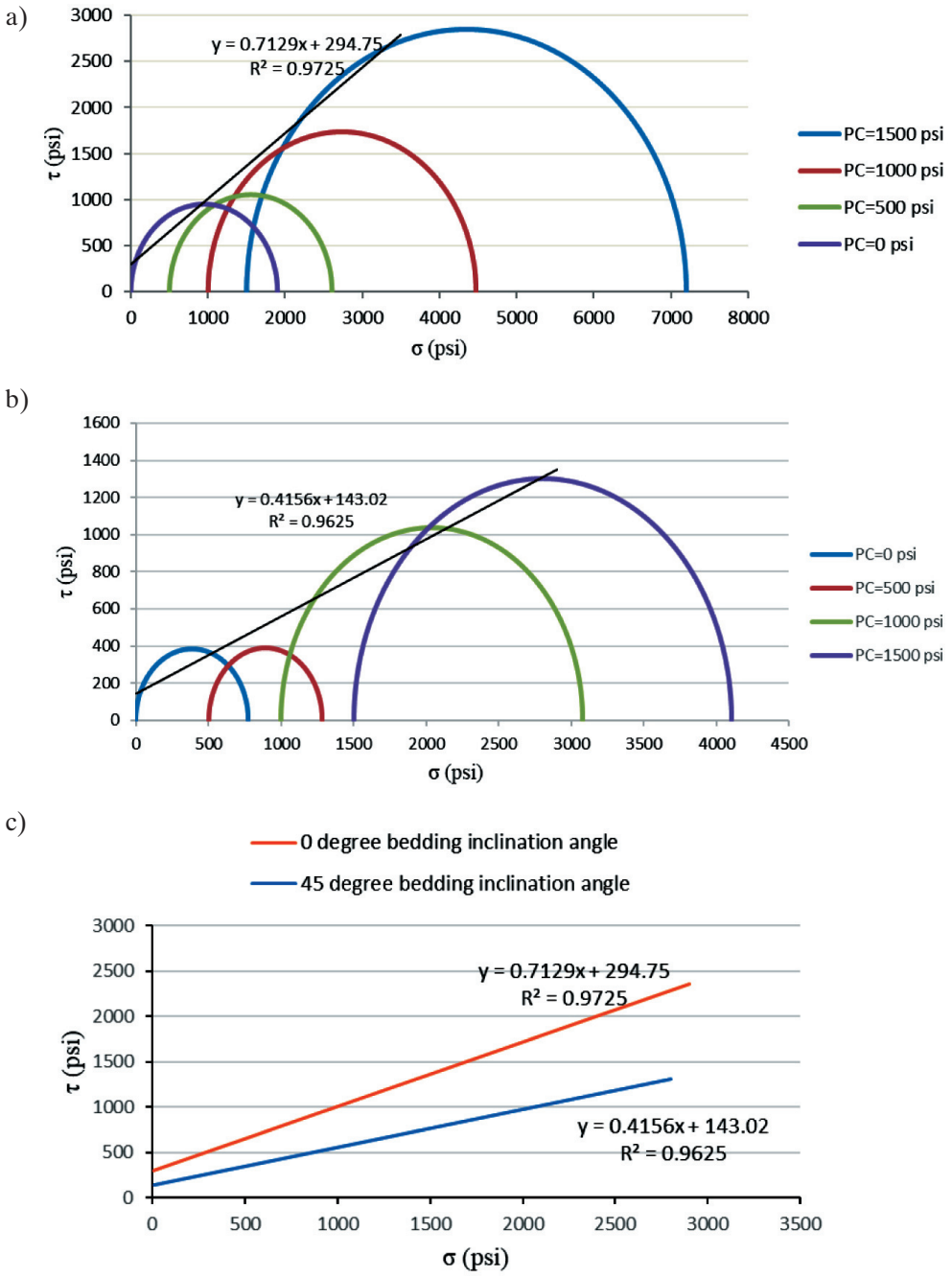

Fig. 13. Failure envelopes: a) for 0 degrees inclination bedding plane;
b) for 45 degrees inclination bedding plane;
c) of plane of weakness failure criterion

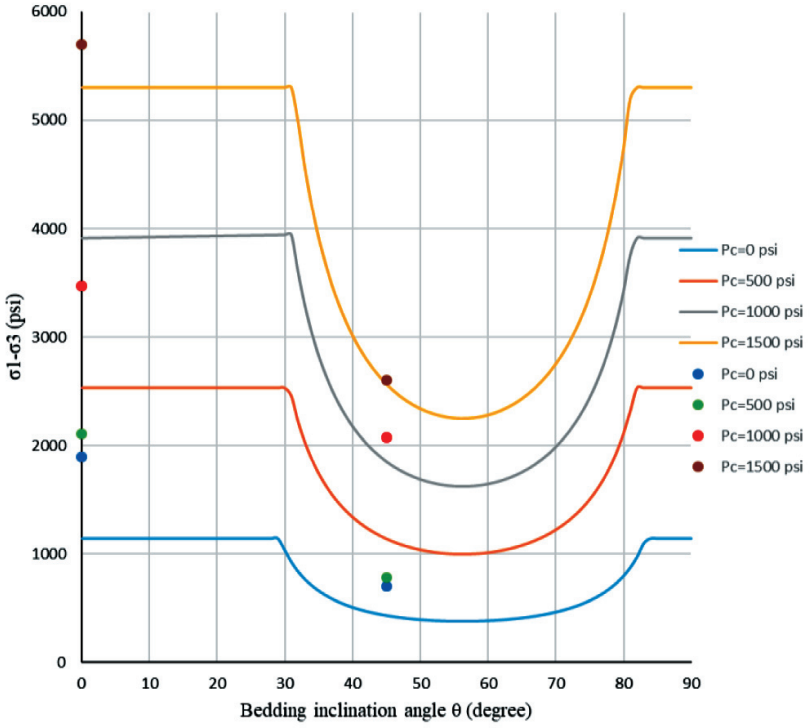

Fig. 14. Plane of weakness criteria

Table 3

Application of SPWM Failure Criterion on Different Cement Systems

Bedding inclination angle [degree]	Cohesion [psi]	Inter friction angle [degree]	Real failure pressure with Pc = 500 [psi]	Real failure pressure with Pc = 1000 [psi]	Real failure pressure with Pc = 1500 [psi]	R^2	RMSE
0	294.75	35.49	2 607	4 473	7 199	0.9725	306.75
45	143.02	22.57	1 280	3 074	4 100	0.9625	38.86

Modified Cam–Clay model

Figure 15 shows the MCCM failure envelope for Trinidad shale. The different stress paths under different confining pressures for strength prediction are also plotted.

The data of material constants, the R-squared and RMSE are presented in Table 4.

Analyzing the R-squared values and RMSE of two failure criteria mentioned above, we conclude that Simple Plane of Weakness and Modified Cam–Clay failure criterion

are both suitable to estimate shale anisotropic. However, the Modified Cam–Clay Model is better than the Simple Plane of Weakness model, because of its high R-squared value and low RMSE.

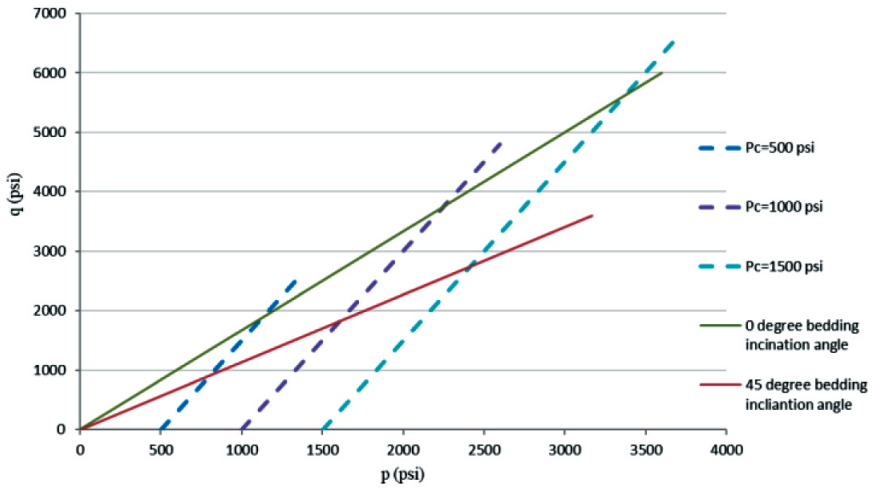

Fig. 15. Modified Cam–Clay Model failure envelope and stress paths for strength prediction

Table 4

Application of MCCM Failure Criterion on Different Cement Systems

Bedding inclination angle [degree]	Slope of critical state line	Real failure pressure with Pc = 500 [psi]	Real failure pressure with Pc = 1000 [psi]	Real failure pressure with Pc = 1500 [psi]	R^2	RMSE
0	1.6654	2 607	4 473	7 199	0.9959	40.99
45	1.1346	1 280	3 074	4 100	0.9916	34.87

5. WELL LOGGING INTERPRETATION

5.1. Parameters in stiffness tensor

Since we have calculated all the elastic parameters for the Trinidad shale by the triaxial test, P-wave velocity at any inclination angle can be evaluated. Figure 16 shows the calculated compressional wave velocity versus different inclination angles. We notice that the P-wave velocity is increasing as bedding inclination angle increases.

We obtained the real logging data of the compressional wave velocity and well inclination angle from the field. Inclination of the shale formation is 42.91 degrees. Accordingly, we calculated the compressional wave velocity by using the elastic parameters in the stiffness tensor from previous experimental result.

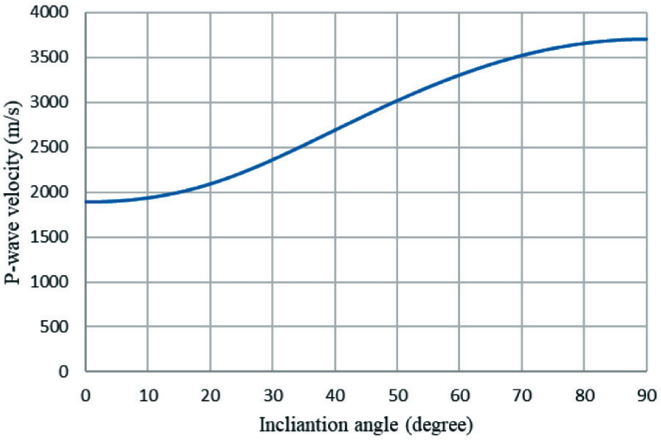

Fig. 16. Compressional wave velocity versus different inclination angles

Table 5 illustrates the difference between the field logging data and the experimental prediction data for our shale. We computed the percent error for velocity, and the error rate was acceptable for primary estimation.

Table 5

Field logging data and experimental prediction data

Δt from field data [μs/ft]	112.87
Δt from prediction [μs/ft]	109.27
P-wave velocity from field data [m/s]	2 700.45
P-wave velocity from prediction [m/s]	2 789.39
Percentage error for velocity [%]	3.29

In summary, calculating the P-wave velocity from the stiffness tensor is a reasonable way to connect the experimental data and field data. In real drilling processes, if we have several wells penetrated through the same formation at different inclination angles, we could estimated the compressional wave velocity of different well inclination angles by inverse calculation. To do the inversion, we need at least three wells of different inclination angles. The process for using sonic log data inversion method to predict the compressional wave velocity of different well inclinations is shown in Figure 17.

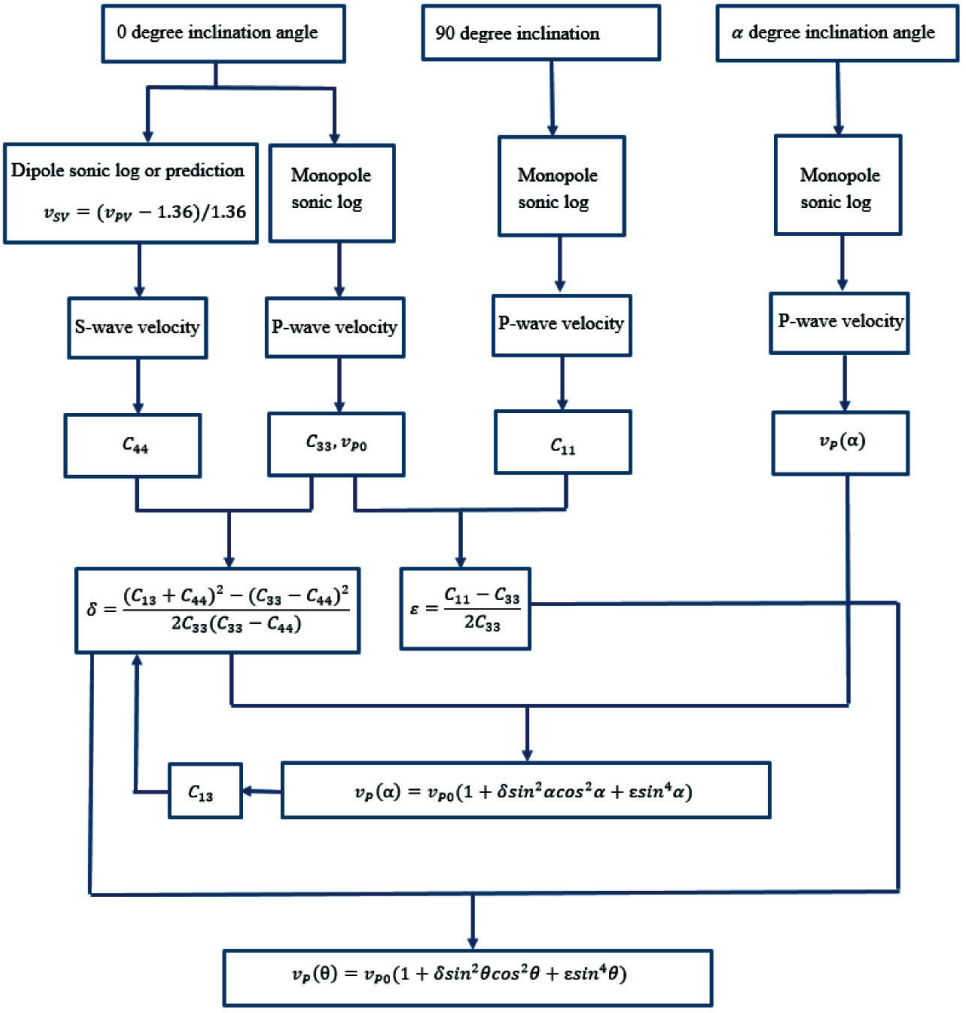

Fig. 17. Inversion method to predict compressional wave velocity at any well inclination

5.2. Uniaxial compressive strength

Generally, the unconfined compressive strength (UCS) and the angle of internal friction (φ) are used for evaluating the minimum mud density during drilling processes. The easiest way to obtain UCS and φ is to perform triaxial tests on cylindrical samples. However, in real practice, shale cores are not always available. As a practical and economic way to obtain the value of UCS and φ, many empirical relations have been proposed.

We have the well logging data for bedding inclination angle of 42.9 degrees. Thus, we used the empirical correlations which contain compressional wave velocity for the anisotropic strength prediction. Table 6 shows the predicted UCS by using compressional wave velocity.

Table 6

Failure tests of different inclination angles (0 degrees and 45 degrees)

Empirical UCS correlation [MPa]	UCS of 0 degrees bedding inclination angle [psi]		Predicted UCS of 45 degrees bedding inclination angle [psi]	
	Prediction	Experiment	Prediction	Experiment
$0.77(304.8/\Delta t)^{2.93}$	724	1 900	2 407	807
$0.43(304.8/\Delta t)^{3.2}$	481	1 900	1 791	807
$1.35(304.8/\Delta t)^{2.6}$	1 028	1 900	2 995	807
$0.5(304.8/\Delta t)^{3}$	491	1 900	1 688	807
$10(304.8/\Delta t - 1)$	1 294	1 900	2 683	807

By comparing the predicted uniaxial compression strength value by well logging data and real experiment result, we can reasonably arrive at the conclusion that prediction of compressional strength by sonic logging data is misleading. However, if well logging data is the only information which we could acquire in a real drilling process, we need to estimate the UCS strength in a conservative way.

6. SHALE ANISOTROPIC STRENGTH FOR MINIMUM DRILLING MUD PREDICTION

For our case, we assumed vertical depth was 5100-ft and vertical pressure gradient was 1 psi/ft. The far-field horizontal stress was estimated to be 3000 psi. Pore pressure was assumed to be 1500 psi. To calculate safety mud window, we followed the flow chart in Figure 18. For our calculation, we used the data predicted by the Simple Plane of Weakness model as input. Figure 19 shows the safety mud density for our case.

Firstly, we notice that the heavier mud is needed for the hole inclination angle in the range: 33.5 degrees to 77.5 degrees. Figure 19 clearly indicates that hole inclination angle higher than about 41 deg is not possible without wellbore strengthening materials.

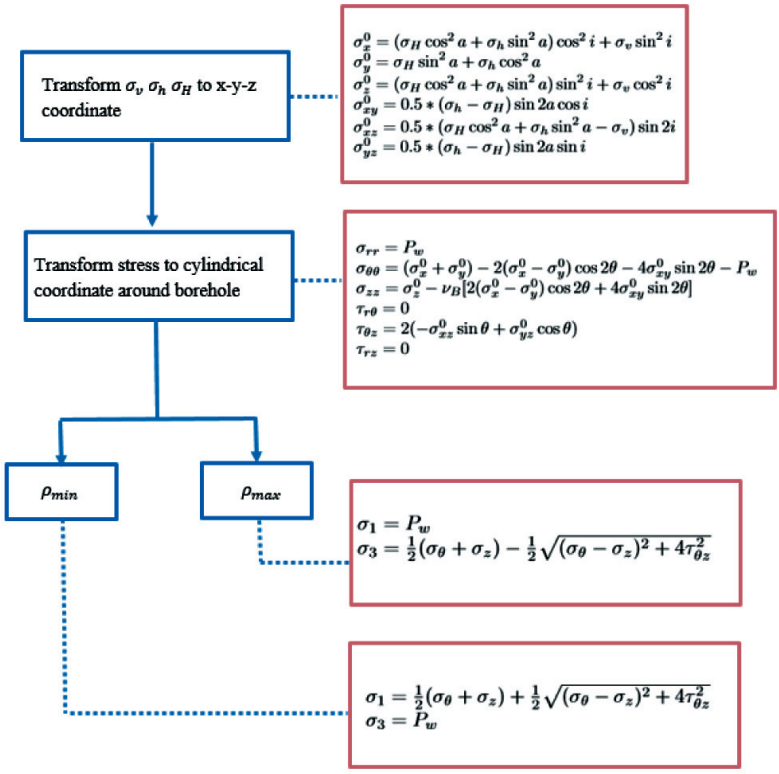

Fig. 18. Flow chart of safety mud window calculation

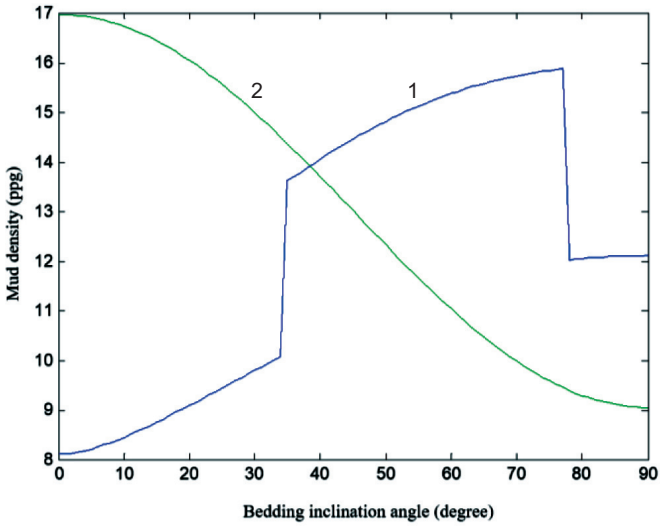

Fig. 19. Safety mud window with respect to well inclination angle:
1 – minimum reguired mud density; 2 – maximum allowable mud density

7. CONCLUDING REMARKS

Based on the experimental results, the following conclusions can be drawn:

Vertical Young's modulus for most of shale rocks is smaller than horizontal Young's modulus. This means that the mechanical strength resistance parallel to the bedding plane is larger than that perpendicular to the bedding plane.

Young's modulus of 0 degrees bedding inclination angle shale sample will increase as the confining pressure increases. However, the increment of confining pressure shows little influence on 45 degrees bedding inclination angle sample.

For same bedding inclination angle, the higher confining pressure the higher compressive strength. Meanwhile, compressive strength of 0 degrees bedding inclination angle sample is always higher than that of 45 degrees bedding inclination angle sample under same confining pressure.

The Simple Plane of Weakness Model and the Modified Cam–Clay failure criterion are both suitable to estimate shale anisotropic compressive strength.

Based on the well logging data interpretation, the following conclusions can be drawn:

To calculate the P-wave velocity from the stiffness tensor is a reasonable way to connect the experimental data and field data. P-wave velocity is increasing as the bedding inclination angle increases.

In drilling process, P-wave velocity and the stiffness parameters can be estimated by inverse calculation. Sonic logging data with different well inclination angles is an input.

Comparing the predicted uniaxial compression strength value by well logging data and real experimental results, prediction of the uniaxial compressional strength by sonic logging data is misleading. If sonic logging information is the only accessible data, we need to use the empirical correlations conservatively.

REFERENCES

[1] Lal M.: *Shale Stability: Drilling Fluid Interaction and Shale Strength*. Paper SPE 154356 presented at the 1999 SPE Annual Technical Conference and Exhibition, Caracas, Venezuela, 21–23 April 1999.

[2] Mehdi M., Mehdi H., Tutuncu A.N.: *Acoustical and Geomechanical Characterization of Eagle Ford Shale – Anisotropy, Heterogeneity and Measurement*. Paper SPE 170707 presented at the 2014 SPE Annual Technical Conference and Exhibition, Amsterdam, The Netherlands, 27–29 October 2014.

[3] Mehdi M., Tutuncu A.N., Kazemi H.: *Integrated Study on Tensile Fracture Mechanics and Subsequent Flow in Naturally Fractured Niobrara Shale*. Paper ARMA 147126 at the 2014 US Rock Mechanics/ Geomechanics Symposium, Minneapolis, USA.

[4] Mokhtari M., Alquhtani A.A., Tutuncu A.N.: *Stress-dependent Permeability Anisotropy and Wettablility of Shale Resources*. Paper SPE 168672 presented at the 2013 SPE Annual Technical Conference and Exhibition, Denver, USA, 12–14 August 2013.

[5] Thomsen L.: *Weak Elastic Anisotropy*. Geophysics, vol. 51(10), 1986, pp. 1954–1966.

[6] Vernik L., Nur A.: *Ultrasonic Velocity and Anisotropy of Hydrocarbon Source Rocks*. Geophysics, vol. 57(5), 1992, pp. 727–735.

[7] Wang Z.: *Seismic Anisotropy in Sedimentary Rocks*. Geophysics, vol. 67(5), 2002, pp. 1423–1440.

[8] Tutuncu A.N.: *The Role of mechanical, acoustic and permeability anisotropies on reservoir characterization and field development for two North American Fractured Unconventional Shale Reservoirs*. Paper ARMA 12644 at the 2012 US Rock Mechanics/ Geomechanics Symposium, Chicago, USA.

[9] Safda K., Sajjad A., Hongxue H.: *Importance of Shale Anisotropy in Estimating Insitu Stresses and Wellbore Stability Analysis in Horn River Basin*. Paper SPE 149433 presented at the 2011 SPE Annual Technical Conference and Exhibition, Calgary, Canada, 14–17 November 2011.

[10] Chang C., Zoback M.D., Khaksar A.: *Empirical Relations between Rock Strength and Physical Properties in Sedimentary Rocks*. Journal of Petroleum Science and Engineering, vol. 51, 2006, pp. 233–237.

[11] Horsrud P.: *Estimating Mechanical Properties of Shale from Empirical Correlations.* Paper SPE 56017-PA, SPE Drilling & Completion, vol. 16(2), 2001.

[12] Voigt W.: *Lehrbuch der Kristallphysik*, 1910. Leipzig etrived, Nov. 29, 2016.

[13] Jaeger J.C. et al.: *Deformation and Failure of Rocks.* [in:] *Fundamentals of Rock Mechanics*, 4th ed., Blackwell Publishing 2007.

[14] Donath F.A.: *Experimental Study of Shear Failure in Anisotropic Rocks*. Geological Society of America Bulletin, vol. 72, iss. 6, 1961, p. 985.

[15] Hoek E.: Fracture of Anisotropic Rock. *Journal of the South African Institute of Mining and Metallurgy*, vol. 64, iss. 10, 1964, pp. 501–518.

[16] Jaeger J.C.: *Fracture of Rocks*. Tewksbury Symposium on Fracture, 1963, pp. 268–283.

[17] Roscoe K.H., Burland J.B.: *On the Generalized Stress-Strain Behavior of 'Wet' Clays*. [in:] Heyman J., Leckie F. (Eds.) *Engineering Plasticity*, Cambridge University 1963, pp. 535–609.

[18] Been K., Jefferies M.G., Hachey J.E.: *The Critical State of Sands*. Geotechnique, vol. 41, iss. 3, 1991, pp. 365–381.

[19] Coop M.R.: *The Mechanics of Uncommented Carbonate Sands*. Geotechnique, vol. 40, 1990, pp. 607–626.